Micromachines **2014**, *5*, 1034-1050; doi:10.3390/mi5041034

OPEN ACCESS

micromachines

ISSN 2072-666X

www.mdpi.com/journal/micromachines

Article

Analysis of Dynamic Performance of a Kalman Filter for Combining Multiple MEMS Gyroscopes

Liang Xue [1,*], Lixin Wang [1], Tao Xiong [1], Chengyu Jiang [2] and Weizheng Yuan [2]

[1] Xi'an Research Inst. of Hi-Tech, Hongqing Town, Xi'an 710025, China; E-Mails: wlxxian@sina.com (L.W.); bbear2@163.com (T.X.)

[2] MOE Key Laboratory of Micro and Nano Systems for Aerospace, Northwestern Polytechnical University, 127 Youyi West Road, Xi'an 710072, China; E-Mails: jiangcy@nwpu.edu.cn (C.J.); yuanwz@nwpu.edu.cn (W.Y.)

External Editors: Stefano Mariani and Joost Lötters

* Author to whom correspondence should be addressed; E-Mail: xuelmems@163.com; Tel./Fax: +86-29-8474-1536.

Received: 25 August 2014; in revised form: 14 October 2014 / Accepted: 31 October 2014 / Published: 7 November 2014

Abstract: In this paper, the dynamic performance of a Kalman filter (KF) was analyzed, which is used to combine multiple measurements of a gyroscopes array to reduce the noise and improve the accuracy of the individual sensors. A principle for accuracy improvement by the KF was briefly presented to obtain an optimal estimate of input rate signal. In particular, the influences of some crucial factors on the KF dynamic performance were analyzed by simulations such as the factors input signal frequency, signal sampling, and KF filtering rate. Finally, a system that was comprised of a six-gyroscope array was designed and implemented to test the dynamic performance. Experimental results indicated that the 1σ error for the combined rate signal was reduced to about 0.2°/s in the constant rate test, which was a reduction by a factor of more than eight compared to the single gyroscope. The 1σ error was also reduced from 1.6°/s to 0.48°/s in the swing test. It showed that the estimated angular rate signal could well reflect the dynamic characteristic of the input signal in dynamic conditions.

Keywords: microelectromechanical systems (MEMS) gyroscope; array signal; filtering; dynamic performance; noise reduction

1. Introduction

Although there is still a great distance between the accuracy of microelectromechanical systems (MEMS) vibratory gyroscopes and traditional gyroscopes such as the fiber-optics gyroscopes, MEMS gyroscopes have recently received more and more attention because of their low cost, small device size, low power consumption, and high reliability combined with ease of fabrication in large numbers on a single wafer [1,2]. MEMS gyroscopes are important components of inertial measurement units (IMU) and are applicable in many sectors such as vehicle navigation, automotive applications, and rollover detection or consumer electronics [3–6]. To date, low accuracy is one of the biggest bottlenecks in development of the MEMS gyroscope, which limits its applications requiring high-precision angular rate signals such as navigation and guidance. Recently, some researchers have explored the possibility to design an array structure of MEMS gyroscopes to improve the signal-to-noise ratio and sensitivity of the device [7,8], in which the sense units are connected to increase the overall detective capacity. Wang *et al.* [7] designed a gyroscope array, which combines several gyroscope cells by using a unique detection mass to increase the gain of sense-mode and improve the system sensitivity. Fortunately, the technology of multi-signal fusion for the gyroscope array is becoming an effective approach to reduce the measurement noise and improve the accuracy of the MEMS gyroscope [9–11], which is called the technology of virtual gyroscope [11]. Its principle lies in several gyroscopes with the same specification that can be combined with each other to form a sensor array and fuse multiple outputs to obtain an optimal rate estimate with a filtering technique.

Signal processing of the gyroscopes array with an optimal estimate algorithm makes it possible to demonstrate significant improvements in measuring angular rates. It was developed to reduce noise and decrease bias drifts existing in the single gyroscopes. In the year of 2003, Bayard and Ploen first proposed the technology of virtual gyroscopes [11]. Previously, an integrated MEMS gyroscope array had been presented by three separate sensors, and a two-level optimal filtering scheme was designed to reduce the bias drift [12]. Additionally, a virtual gyroscope that was composed of a six-gyroscope array was designed [13]. The factors that affected the accuracy improvement were analyzed in detail. Particularly, the influence of correlation factors on the accuracy improvement was evaluated. The results indicated that the performance of the Kalman filter (KF) was better than that of the arithmetic averaging process. In addition, an approach for combining multiple uncorrelated MEMS gyroscopes was presented to improve the accuracy [14]. A KF was designed to fuse the outputs of the several uncorrelated sensors, and the improvement was better than that of an averaging process under certain conditions.

Recently, the redundant MEMS IMUs have been utilized to improve navigation performance. Numerous studies have been undertaken on redundant IMU integration [15,16], into what can be called a virtual IMU (VIMU). In [15], three mechanization approaches of the system and an observation model for the multiple IMUs integration were described. In [16], an approach for reducing the noise of the inertial sensors was studied by using multiple MEMS IMUs; furthermore, the inertial navigation system (INS)/global positioning system (GPS) integrator based on the synthetic IMU, extended IMU, and geometrically constrained IMU mechanization were presented for integration of GPS with redundant MEMS-IMUs. It was shown that the idea of a virtual gyroscope is essentially identical with the VIMU, since both of them fuse multiple measurements to create a combined signal for improving performance. Additionally, some important studies are carried out to analyze the stochastic modeling of IMU to

enhance the performance of INS/global navigation satellite systems (GNSS) [17,18]. Usually, the error features and the INS error calibration model of an IMU depend on the environmental conditions that mainly include temperature and dynamics. A method for IMU error analysis was proposed in [17], which consisted of using a reference IMU together with the IMU under test for the simultaneous measurement of two IMU signals. The relationship between the IMU errors and motion dynamics was investigated as well. In [18], an estimator based on the Generalized Method of Wavelet Moments (GMWM) was presented. It applied the GMWM on error signals from MEMS inertial sensors by building and estimating composite stochastic processes, which could solve the problem of identifying correct error-state parameters of inertial sensors when several stochastic processes were superposed.

For the creation of a gyroscope array, the dynamic performance of the KF is a key factor to improve the overall accuracy of the gyroscope in a dynamic condition. However, the previous reported virtual gyroscope approaches [11–14] primarily focused on the analysis and evaluation of noise reduction in a static condition. Unfortunately, few of the previous works have analyzed the dynamic performance of KF. Furthermore, the output of a MEMS gyroscope is widely modeled as a summation of the true angular rate signal and random noise. The terms of the random noise are determined by the type of sensor and its application environment. The true angular rate signal is directly modeled to obtain an optimal estimate—this is the foundation and prominent characteristic of the virtual gyroscope technology. However, as for such modeling, the dynamic performance of KF is heavily related to designing parameters such as noise variance driving for true angular rate signal and KF filtering rate. In this study, the dynamic performance of a virtual gyroscope is evaluated, furthermore, the influence of noise variance for driving true angular rate signals, input signal frequency, signal sampling rate, and KF filtering rate on the performance improvement is also studied. The research provides a useful basis and guidance for practical system implementation and application.

This paper is organized as follows. In Section 2 the principle model of the virtual gyroscope is briefly described. In Section 3 the dynamic performance of the virtual gyroscope is analyzed. In Section 4 the dynamic performance is verified by various simulations. In Section 5 some dynamic experiments are conducted including constant rate and swinging rate tests in the turn-table. Lastly, some conclusions are drawn.

2. Principle Model of the Virtual Gyroscope

The output of the gyroscope is corrupted by some typical errors such as bias, drift, and scale factor error [19]. Hence, a general gyroscope measurement model can be formed as follows:

$$\begin{cases} y(t) = (1 + g_{sf})\omega(t) + b_0 + b(t) + n(t) \\ \dot{b}(t) = w_b(t) \end{cases} \quad (1)$$

where y is the measured angular rate, ω is the true angular rate, b_0 is the bias, w_b is the rate random walk (RRW) white noise, b is the bias drift driven by noise w_b, $n(t)$ is the angular random walk (ARW) white noise, and g_{sf} is the scale factor error. The bias b_0 is a constant offset from the sensor's output, which can be determined and compensated through averaging the long-term data acquired from the sensor output subjected to zero input. The scale factor error g_{sf} will seriously affect the outputs of MEMS gyroscope during a high rate maneuvering.

In this paper, bias b_0 can be known through averaging the long-term data. For MEMS gyroscopes with a lower accuracy, numerous experiments have demonstrated that the RRW and ARW are considered the most dominant error sources. The results in [20] demonstrated that the ARW is a dominant error in the short cluster time, whereas the bias drift term is the dominant error in the long cluster time. The RRW term will affect the long-term accuracy of the MEMS gyroscope. In this paper, the scale factor error can be removed from the general measurement Equation (1) because of the lower dynamic environment. With a short time application, the bias drift can be ignored. Therefore, to reduce the dimension of KF and estimate the true angular rate signal from the gyroscope's measurement, a simplified model was taken to describe the gyroscope as:

$$y(t) = \omega(t) + n(t) \tag{2}$$

As for a gyroscope array with a component device number of N, Equation (2) can be expressed in vector form as:

$$\boldsymbol{Z}(t) = \boldsymbol{H} \cdot \omega(t) + \boldsymbol{v}(t) \tag{3}$$

with

$$\boldsymbol{Z}(t) = \left[y_1, y_2, \cdots, y_N\right]^T,\ \boldsymbol{H} = \left[1,1,\cdots,1\right]_{N\times 1}^T,\ \boldsymbol{v}(t) = \left[n_1, n_2, \cdots, n_N\right]^T \tag{4}$$

where y_i is the output of rate signal of the ith gyroscope, $\boldsymbol{Z}(t)$ is the output measurements of the gyroscope array, $\boldsymbol{H}$ is the measurement matrix, n_i is the ARW white noise of the ith gyroscope, $\boldsymbol{v}(t)$ is the white noise vector with $E[\boldsymbol{v}(t)] = 0$ and $E[\boldsymbol{v}(t)\boldsymbol{v}^T(t+\tau)] = \boldsymbol{R}\delta(\tau)$, representing system measurement noise, and $\boldsymbol{R}$ is the covariance matrix of the noise vector $\boldsymbol{v}(t)$.

In order to get a considerable noise reduction, the true angular rate signal is modeled to design a KF. Here, the true angular rate signal is described by a process of random walk driven by a zero-mean white noise n_ω [13]:

$$\dot{\omega} = n_\omega \tag{5}$$

where n_ω is a zero-mean white noise with $E[n_\omega(t)n_\omega^T(t+\tau)] = q_\omega\delta(\tau)$, and q_ω is the variance of white noise n_ω. Using a KF technique, setting the true angular rate ω as the system estimated quantity, based on the gyroscope model of Equation (3) and true angular rate model of Equation (5), thus the filtering state-space model for virtual the gyroscope system can be expressed as:

$$\begin{cases} \dot{X}(t) = F \cdot X(t) + w(t) \\ \boldsymbol{Z}(t) = \boldsymbol{H} \cdot X(t) + \boldsymbol{v}(t) \end{cases} \tag{6}$$

where KF system state is $X(t) = \omega$, the coefficient scalar $F = 0$, and the system process noise $w(t) = n_\omega$ with $E[w(t)w^T(t+\tau)] = q_\omega\delta(\tau)$.

Based on Equation (6), the continuous KF for the true angular rate estimate can be given as:

$$\dot{\hat{X}}(t) = \boldsymbol{K}(t)\left[\boldsymbol{Z}(t) - \boldsymbol{H}\hat{X}(t)\right] \tag{7}$$

$$\boldsymbol{K}(t) = P(t)\boldsymbol{H}^T\boldsymbol{R}^{-1} \tag{8}$$

$$\dot{P}(t) = q_\omega - P(t)\boldsymbol{H}^T\boldsymbol{R}^{-1}\boldsymbol{H}P(t) \tag{9}$$

where $\hat{X}(t)$ is the estimate of the system state, $\boldsymbol{K}(t)$ is the filter gain, and $P(t)$ is the estimated covariance. Previously, an analytic approach was used to solve the continuous-time KF from Equation (7) to Equation (9) in [13], and led to a steady-state covariance and gain, thus the discrete-time KF for rate signal estimate can be given as:

$$\hat{X}_{k+1} = e^{-\sqrt{Cq_\omega}T}\hat{X}_k + C^{-1}(1-e^{-\sqrt{Cq_\omega}T})\boldsymbol{H}^T\boldsymbol{R}^{-1}\boldsymbol{Z}_{k+1} \tag{10}$$

where $C = \boldsymbol{H}^T\boldsymbol{R}^{-1}\boldsymbol{H}$, and T is the filtering period. Hence the true angular rate signal can be estimated and obtained by the discrete-time KF of Equation (10).

If we define the parameter $\alpha = \exp(-\sqrt{Cq_\omega}T)$ and the matrix $Q = C^{-1}\cdot(1-\alpha)\cdot H^T R^{-1}$ (here β is the component values of the matrix Q), then the discrete-time KF of Equation (10) can be expressed as:

$$\hat{X}_{k+1} = \alpha\cdot\hat{X}_k + \beta\cdot[1,1,\cdots,1]_{1\times N}\cdot\boldsymbol{Z}_{k+1} \tag{11}$$

Therefore, the parameters α and β can be regarded as the KF weight factor corresponding to the estimated value $\hat{X}_k$ and system measurement $\boldsymbol{Z}_{k+1}$, which satisfies the relationship of $\alpha + N\cdot\beta = 1.0$. Equation (11) shows that the values of factors α and β are mainly determined by the parameter q_ω. The expression of factor α indicates that the value of α is a negative exponential function with parameter $\sqrt{q_\omega}$, thus it will quickly decrease with increasing q_ω, and eventually it will approach zero while q_ω increases to a larger value. On the contrary, factor β will increase with increasing q_ω, and eventually approach to $1/N$. In this case, the performance of KF will be comparable with that of an arithmetic averaging process.

It can be seen in Equations (5) and (10) that the true angular rate signal is modeled directly to obtain an optimal estimate. The advantage of this lies in that a complete state-space model for KF can be designed and an optimal estimate of the true angular rate can be directly obtained using a KF technique. Furthermore, the performance of KF and accuracy of a combined rate signal can be analyzed by the covariance $P(t)$, providing a basis for parameter adjustment. However, the random walk process as described in Equation (5) cannot always be used to accurately represent and reflect the practical characteristics of the input rate signal, especially in a high dynamic condition. However, practically, if the input rate signal has a small variation or is nearly constant, the true angular rate signal could be modeled with a small driven white noise variance q_ω. If the input rate has a more dynamic behavior, the true angular rate signal can be modeled with a larger driven white noise variance q_ω. Thus, the variance q_ω can be used to set a different KF bandwidth to satisfy the requirement of dynamic characteristics.

In the designing of KF, the number N of individual gyroscopes in the array can be chosen as any integer. Due to the characteristics of MEMS technology, it can design and fabricate multiple sensor arrays in a small size. Therefore, the focus of this paper is not on the geometrical layout of the gyroscope array. Furthermore, the performance of a virtual gyroscope can be evaluated by $P(t)$ since it represents the estimated variance of the state vector $X(t)$ [13]. Previous work in [13] demonstrates that the noise reduction can be increased and the performance of KF can be further improved by increasing the number of N. However, it should try to select the components of the gyroscope that have the same specification to construct a sensor array, thus one needs to consider the sensor array complexity and uniformity between the component gyroscopes. In this paper, the six-gyro array ($N = 6$) is selected to construct the virtual gyroscope and analyze the performance. It should be noted that $N = 6$ is really not an optimal choice, it is only chosen to analyze the dynamic performance of the KF.

3. Dynamic Performance Analysis of Virtual Gyroscope

In our previous studies [13], a steady-state covariance $P_\infty(t)$ was obtained using an analytic solution. Furthermore, the relationship between the correlation factors among the cells of the sensor array and the noise reduction was analyzed in detail. Here we will focus on the dynamic characteristics analysis of the virtual gyroscope system.

3.1. Analysis of KF Weight Factor on Performance

The discrete-time KF of Equation (11) indicates that the rate estimate $\hat{X}_{k+1}$, *i.e.*, $\hat{\omega}_{k+1}$ for the time point t_{k+1} is composed of two parts, *i.e.*, the rate estimate $\hat{X}_k$ for the time point t_k and the outputs of gyroscope array $\boldsymbol{Z}_{k+1}$ at t_{k+1} time point, the weight of which are determined by the factors α and β. With the sensors number of $N = 6$, the assumption is made that the ARW noise for the single gyroscope is $6.3°/\sqrt{h}$ and the sampling rate is set to 200 Hz. When using the expression of α and β, the values of α and β *versus* a different parameter q_ω are plotted in Figure 1.

Figure 1. Plot of Kalman filter (KF) weight factors *versus* different values of $\sqrt{q_\omega}$.

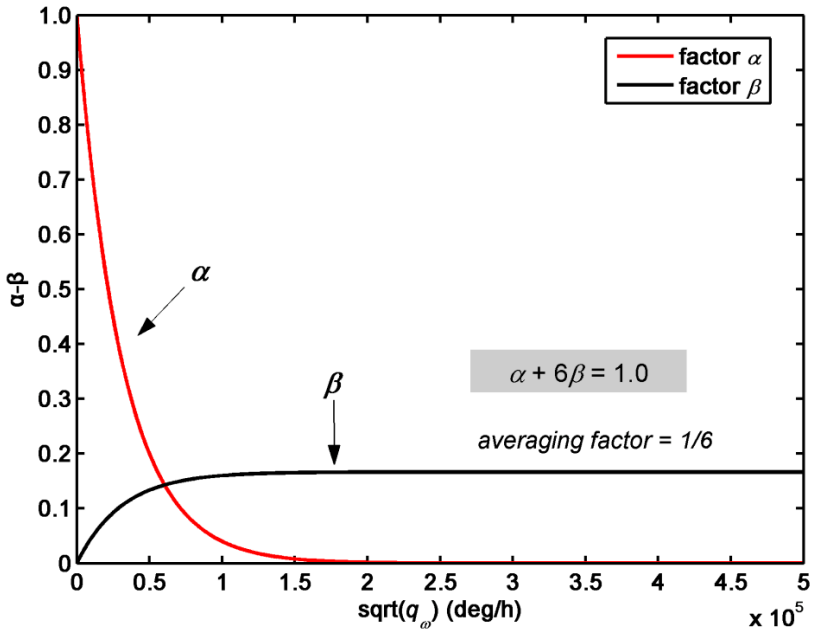

Figure 1 shows that the factors α and β vary with q_ω. In particular, factor α decreases and factor β increases when q_ω is increased. Furthermore, the values of α are bigger than those of β when q_ω is located within a small range, now $\hat{X}_k$ will dominate the values of $\hat{X}_{k+1}$ compared to the $\boldsymbol{Z}_{k+1}$. In this case, the performance of KF is higher than that of an averaging process. The factor α will converge to zero and β will approach an averaging effect factor of 1/6 with increasing values of q_ω, at this point the output of the KF $\hat{X}_{k+1}$ entirely depends on the measurements of $\boldsymbol{Z}_{k+1}$, and it is approximately equal to the effect of an averaging process. Therefore, by analyzing the KF weight factor, the KF dependency on the estimated value $\hat{X}_k$ and measurement value $\boldsymbol{Z}_{k+1}$ can be observed directly. Meanwhile, the relationship between the performance of KF and a simple averaging process is revealed, providing a basis for choosing the system designing parameters.

3.2. Analysis of Sampling and Filtering Rate on Accuracy Improvement

In Section 2, the true angular rate signal ω is modeled as a random walk driven by a white noise n_ω, *i.e.*, $\dot{\omega}(t) = n_\omega$, thus the discrete-time model for describing the true angular rate signal can be expressed as:

$$\omega_{k+1} = \omega_k + W_k \tag{12}$$

where W_k is a sequence of the white noise n_ω. The transition matrix for the KF system of Equation (6) is $\Phi_{k,k-1} = 1$ due to the $F = 0$. Thus, according to the Equation (12), the KF filtering model of Equations (6) and (10) will be more accurate when the input rate signal is nearly zero or with a constant characteristic, in such a situation, a considerable accuracy improvement can be obtained by the KF. On the contrary, the accuracy improvement would be degraded due to an inexact filtering model when the input rate signals have a high dynamic characteristic, because the variations between the values of the two input rate signals associated with the adjacent time points increase in a high dynamic condition, while the KF model requires a smaller variations. To overcome this problem, the sensors sampling rate and KF filtering rate can be increased to reduce the variations between the values of two input rate signals. In the simulation sections, the influence of the sensors sampling rate and KF filtering rate on accuracy improvement will be analyzed and evaluated.

4. Dynamic Simulation of Virtual Gyroscope

In previous works, the static performance of virtual gyroscope was analyzed and evaluated in [13]. The simulations in this study will focus on analyzing the influence of some factors on the dynamic performance improvement, *i.e.*, frequency of input signal, parameter q_ω, sensors signal sampling, and KF filtering rate. The standard deviation (1σ) of the estimated errors is used to quantify the accuracy before and after KF filtering in the dynamic condition, thus the improvement factor (*IF*) can be defined as:

$$IF = \sigma_{single} / \sigma_{Vg} \tag{13}$$

where σ_{single} is the 1σ error for the component gyroscopes, and σ_{Vg} is the 1σ error of the estimated errors for the virtual gyroscope outputs. The mathematical definition of the 1σ error is defined as:

$$\sigma = \sqrt{\frac{1}{n-1}\sum_{i=1}^{n}(\hat{\omega}_i - \omega_{i,true})^2} \tag{14}$$

where $\hat{\omega}_i$ is the estimate of the true angular rate associated with the *i*th time, and $\omega_{i,true}$ is the true angular rate associated with the *i*th time, and *n* is the length number of samples. The simulink model for discrete-time KF (Equation (10)) is shown as Figure 2.

Figure 2. Simulink filtering model for discrete-time KF.

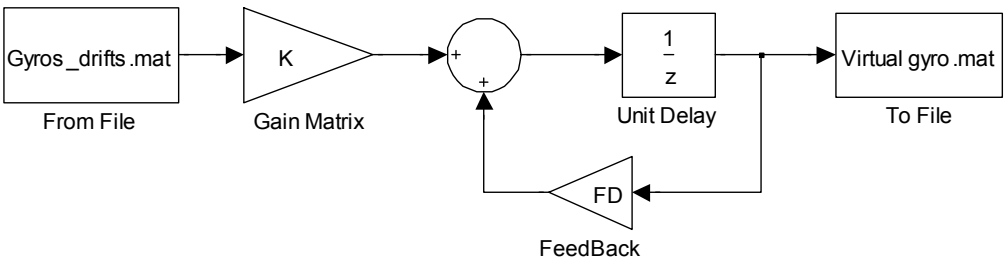

4.1. Influence of Signal Frequency on Dynamic Performance Improvement

The model of a virtual gyroscope shows that the performance of the KF is heavily affected by q_ω. This point had been demonstrated in previous works in [13]. As for a swing input rate signal $\omega = A \cdot \sin(2\pi ft)$ with the frequency f, the improvement factor *IF* will be different with the various choices of q_ω. Concretely, when q_ω is small, the *IF* is lower than one; this implies that there is a large attenuation. In this case, the virtual gyroscope signal cannot accurately reproduce the dynamic behaviors of the input rate signals. As q_ω increases, the *IF* becomes bigger and reaches the maximum value at the specified point corresponding to the optimal $\sqrt{q_\omega}$. After the peak, the *IF* begins to decline and eventually reaches the steady-state value. There exists a peak corresponding to the maximum *IF* during the whole range of parameter q_ω under a frequency f. Consequently, in this work, based on the multiple simulations, we analyze the influence of frequency f on the KF dynamic performance improvement, where f is the frequency of the input swing rate signal. It can be concluded that the maximum improvement factor can be determined and achieved for a dynamic input rate signal having a frequency of f. It can also be found that the maximum improvement factor is different with the various frequency f of the input rate signal. Thus, the relationship between the maximum improvement factor and input signal frequency f will be analyzed.

The input rate signals are generated by the gyroscope model of Equation (2) with a sampling rate of 200 Hz. The ARW noises for the gyroscopes are assumed to be $2.0°/\sqrt{h}$. The true angular rate signal is assumed to be a swing input signal $\omega = A \cdot \sin(2\pi ft)$, with an amplitude of A = 5 and 10°/s, respectively. The frequency f is chosen to be in the range from 0 to 10 Hz. The maximum improvement factor *versus* frequency f is plotted in Figure 3. Note that a specific value of q_ω corresponds to each frequency in Figure 3, by choosing such values, the maximum improvement factor can be obtained, *i.e.*, the optimal q_ω varies with f.

Figure 3. Plot of maximum improvement factor *IF versus* frequency of the input rate signal, f ranges from 0 to 10 Hz.

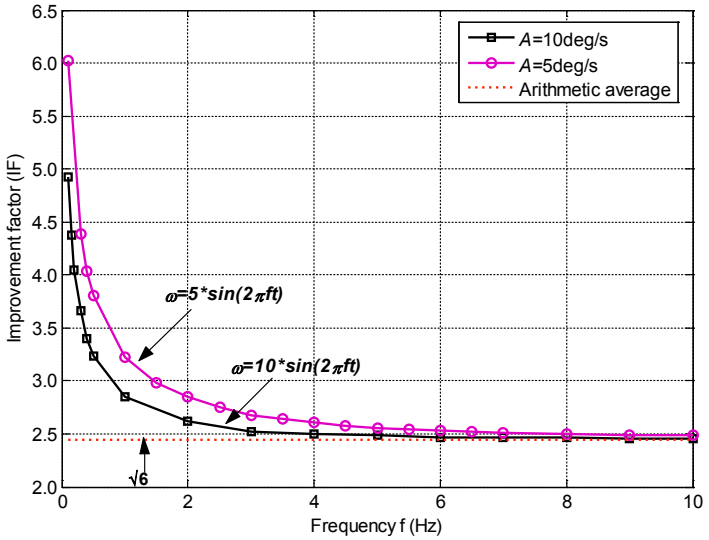

As the graph indicates, the maximum improvement factor decreases with increasing input frequencies f and eventually approaches $\sqrt{6}$. The graph also shows that the improvement factor is higher than $\sqrt{6}$

for the frequency *f* range from 0 to 10 Hz. In addition, it displays a greater slope of the improvement factor for lower input frequencies (0 to 3 Hz) than for higher frequency. Furthermore, the improvement factor obtained by a smaller amplitude (A = 5°/s) is higher than that of the input rate signal with a larger amplitude, this is because the signal's dynamic property is determined by both of the amplitude and frequency.

4.2. Influence of Sampling and Filtering Rate on Accuracy Improvement

As discussed in Section 3.2, the sensors sampling rate and KF filtering rate will affect the accuracy improvement. Firstly, the KF filtering rate will be analyzed. The input rate signals are generated by the Equation (2) with a sampling rate of 500 Hz. The ARW noises for the gyroscopes are assumed to be $4.0°/\sqrt{h}$. The input rate signal is assumed to be a sinusoidal signal of $\omega = A \cdot \sin(2\pi ft)$ with the amplitude A = 30°/s and frequency f = 10 Hz. Three different KF filtering rates are chosen, *i.e.*, f_{KF} = 500, 250, and 100 Hz. For the filtering rate f_{KF} = 250 and 100 Hz, there exist two methods for processing the raw data: (1) Interval average filtering, *i.e.*, calculating the arithmetic average of the input rate signal contained in a filtering period, and then regarding the averaged rate signals as a new measurement sequence for KF processing; (2) Interval sampling filtering, *i.e.*, selecting one of the input rate signals in a filtering period as the new measurement sequences for KF processing. Using the simulink model (Figure 2), the outputs of virtual gyroscope are shown in Figure 4. The detailed results are illustrated in Table 1.

Figure 4. Plot of improvement factor *IF* for various $\sqrt{q_\omega}$ for two different processing methods with filtering rates of f_{KF} = 500, 250, 100 Hz. (**a**) Interval average filtering. (**b**) Interval sampling filtering.

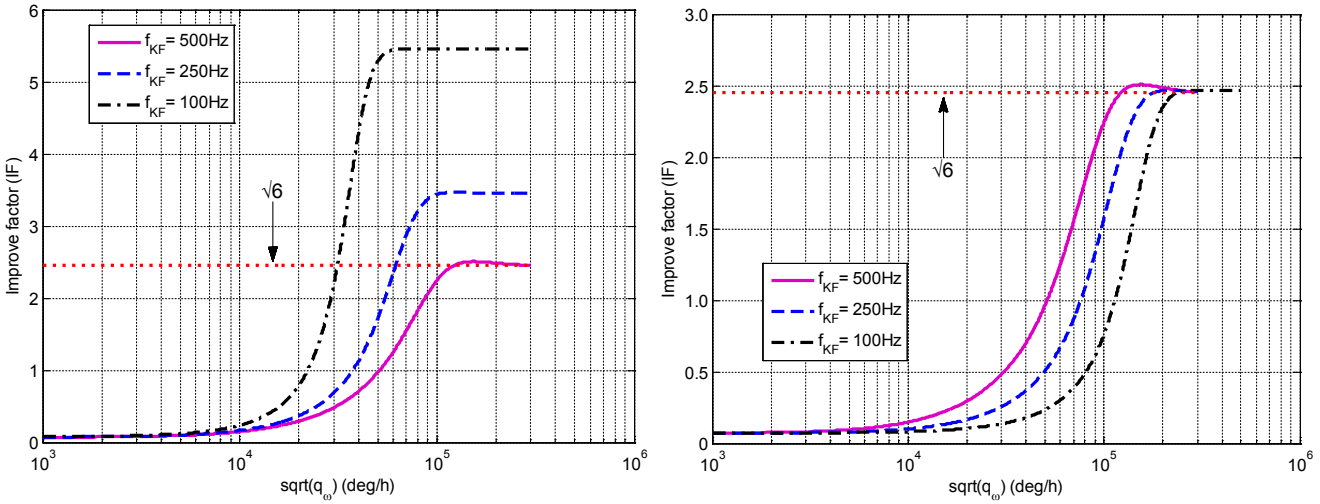

Table 1. Simulation results of a virtual gyroscope with different filtering rates.

Terms	500 Hz	Interval average filtering		Interval sampling filtering	
		250 Hz	100 Hz	250 Hz	100 Hz
Optimal $\sqrt{q_\omega}$ (°/h)	154,900	123,100	76,000	214,300	295,200
Estimated error (1σ, °/s)	0.5946	0.4301	0.2730	0.6044	0.6044
Maximum improvement factor (*IF*)	2.6037	3.4669	5.4612	2.4670	2.4670

The results show that the different filtering rates lead to different performances. Table 1 indicates that the maximum *IF* associated to the filtering rate of 250 Hz and 100 Hz for the interval average filtering are higher than that of 500 Hz. This is because the multiple rate signals are averaged in a filtering period to form a new measurement for KF for the interval average filtering. In particular, the maximum *IF* is found to be approximately $\sqrt{6}\cdot\sqrt{m}$, where m is the number of rate signals that were contained in a filtering period. However, the method of the interval average filtering is not suitable for application having a larger dynamic characteristic. It may result in an inaccuracy of measurements for KF due to the average process, and this inaccuracy will increase with increasing numbers of rate signals in a filtering period. As for the method of interval sampling filtering, the maximum *IF* associated with the filtering rate 250 Hz is 2.467, which is lower than that of 500 Hz, namely 2.6037. The reason lies in that the variations between the values of two input rate signals associated with adjacent time points are increased through interval sampling, resulting in a larger model error than that of the filtering rate f_{KF} = 500 Hz, and eventually degrading the KF performance. Therefore, the KF filtering rate should be set to be the same as the sensors sampling rate to reduce the estimated error.

Secondly, the influence of the sensors sampling rate on KF performance is analyzed. The input rate signal is assumed to be a sinusoidal signal of $\omega = A\cdot\sin(2\pi ft)$, with A = 30°/s and f = 0.25 Hz. Different sampling rates, such as f_s = 100, 200, 250, 500, 1000, 2000, and 3000 Hz, are chosen to collect the sensors signal to evaluate the KF performance. In the KF implementation, the KF filtering rate is set to be the same as the sensors sampling rate, *i.e.*, $f_{KF} = f_s$. Using the simulink model (Figure 2), the relationship between the improvement factor and the sampling rates *versus* different values of $\sqrt{q_\omega}$ is obtained as shown in Figure 5. The detailed results are shown in Table 2.

Figure 5 indicates that the *IF* varies with sampling rates f_s. In particular, it will expand with an increase in the sampling rate and will eventually approach $\sqrt{6}$ with larger values of $\sqrt{q_\omega}$, *i.e.*, the averaging effect. Table 2 indicates that the 1σ error is reduced from 2.9893°/s to 0.7715°/s when the f_s = 100 Hz, which is larger than the result of 0.2738°/s corresponding to the sampling rate 3 kHz. This is because the amplitude variation between the two signals for the adjacent time point becomes smaller with increasing sampling rate, implying that the KF model error is decreased. In addition, the plot also illustrates that the optimal range for $\sqrt{q_\omega}$ located in which the *IF* is higher than $\sqrt{6}$ will be magnified with increasing f_s.

However, from the plot of 1σ estimated errors (Figure 6), it can be seen that graph slope of the 1σ errors gradually becomes smaller with increase of the sensor sampling rate. This means that the decreasing magnitude of the 1σ errors is smaller than that of the increasing magnitude of the sensor sampling rates, and the 1σ errors would not be decreased unlimitedly with the increase of sensor sampling rates. The influence of sampling rate on the reduction of 1σ errors becomes smaller and smaller as the sampling rate increases. Thus some conclusions can be formulated: under the premise of satisfying the requirements of system hardware, the sampling rate should be increased in order to reduce the KF model error with the aim of obtaining a better performance while the input rate signal has a larger dynamic characteristic. On the contrary, a lower sampling rate should be used to reduce the computational load while the input rate signal is nearly constant or has a smaller dynamic characteristic. In addition, the KF filtering rate should be kept at the same value as the sampling rate.

Figure 5. Plot of improvement factor *versus* different values of $\sqrt{q_\omega}$ under different sampling rates f_s = 100, 200, 250, 500, 1000, 2000, 3000 Hz.

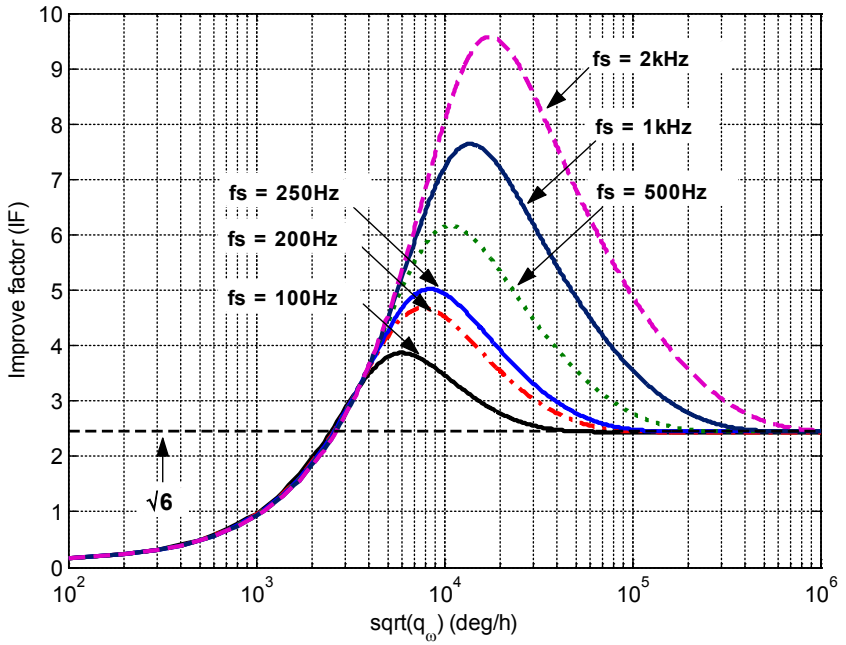

Table 2. Simulation results of virtual gyroscope with different sampling rates.

Sampling rate f_s (Hz)	Estimated error 1σ (°/s)		Maximum improvement factor
	Single gyro	Virtual gyro	
100	2.9839	0.7715	3.8677
200	2.9837	0.6380	4.6766
250	2.9813	0.5941	5.0182
500	2.9812	0.4836	6.1646
1000	2.9807	0.3903	7.6369
2000	2.9820	0.3116	9.5700
3000	2.9802	0.2738	10.8846

Figure 6. Plot of the 1σ estimated errors *versus* the sensor sampling rate.

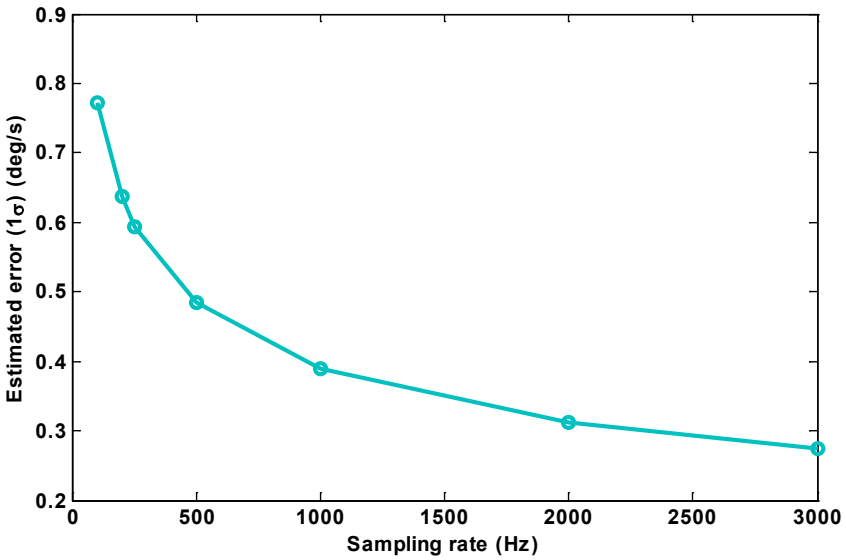

5. Experiments

In this section, the dynamic experiments are carried out to evaluate the performance of KF and quantify the accuracy of the virtual gyroscope signal. The prototype of the designed virtual gyroscope is shown in Figure 7. It is mainly composed of a gyroscope array and a digital signal processing (DSP) unit. Six MEMS gyroscopes ADXRS300 [21] are used to form a gyroscope array; its bandwidth is about 40 Hz. Here, a DSP chip TMS320VC5416 [22] is chosen as the core processor. The A/D data acquisition unit uses a 16-bit ADS7807 [23] to collect voltage signals from gyroscopes array.

The noise statistics of the gyroscope array can be identified and quantified by using the Allan variance technique [20,24]. By using a conventional Allan variance approach in [20] to analyze the data of the component gyroscopes, the results are illustrated in Table 3, where the confidence interval was taken as 90% for estimating the parameters of the gyroscopes. It can be seen that the inconformity of the ARW and bias instability are relatively small for component gyroscopes, thus these component gyroscopes can be regarded as having the same specification and are suitable to form a virtual gyroscope array. The dynamic tests are implemented on a horizontal turntable. The 1σ error is used to evaluate the angular rate signals before and after KF filtering. The improvement factor is also defined by Equation (13). The constant and swing input rate signal tests are chosen to test the virtual gyroscope system.

Figure 7. Prototype of the developed virtual gyroscope system.

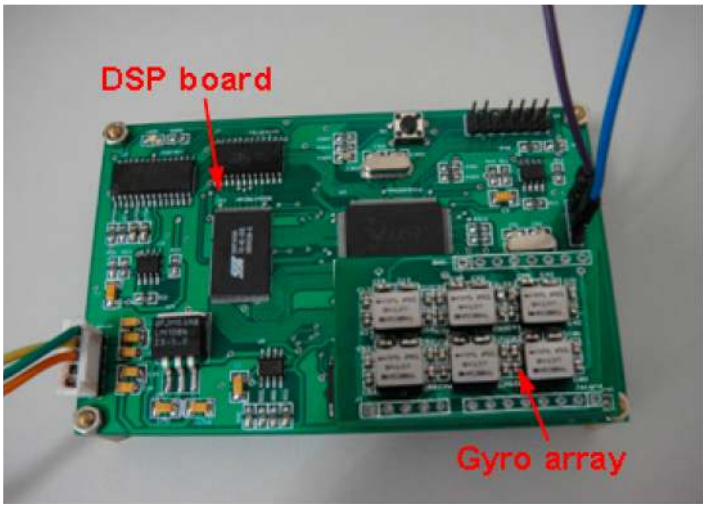

Table 3. Allan variance analyses of component gyroscopes for noise parameters of angular random walk (ARW) and bias instability with associated 90% confidence intervals.

Term	Gyro1	Gyro2	Gyro3	Gyro4	Gyro5	Gyro6
ARW (°/$\sqrt{h}$)	6.3032	6.2308	6.2308	6.3382	6.2845	6.2555
Bias Instability (°/h)	59.2476	58.3598	60.3401	60.1159	57.7861	60.0119

The computational burden is an important issue and should be considered. In this work, a simplified model of Equation (2) was taken to describe the gyroscope and then design the KF algorithm. Finally, a discrete-time KF of Equation (10) for combined rate signal estimate was established. Equation (10) shows that the $e^{-\sqrt{Cq_\omega}T}$ and C are single variables. Hence, the system computation is mainly dependent on the matrix operation of $\boldsymbol{H}^T\boldsymbol{R}^{-1}\boldsymbol{Z}_{k+1}$. Furthermore, the number of N and noise statistics of the

gyroscopes will be determined and fixed while the sensors array is determined. At this time, the covariance matrix R can be determined. Therefore, the value of parameter $e^{-\sqrt{Cq_\omega}T}$ and matrix $C^{-1}(1-e^{-\sqrt{Cq_\omega}T})H^T R^{-1}$ can be calculated off-line in advance, and then these parameters can be written into the program for real-time processing of the information coming from the sensors array, in which case the computational burden becomes a matrix product with the matrix dimensioned of $1 \times N$ multiplied by the matrix dimensioned of $N \times 1$, with computational complexity of only O(N). Thus, a DSP processor could completely satisfy the system requirements of real-time processing.

5.1. Constant Rate Signal Test

Five different constant rates of ω = 10, 30, 50, 80, and 120°/s were given to test the dynamic performance of KF on a turntable. The turntable is controlled to rotate from the static condition. The outputs of the virtual gyroscope are shown in Figure 8. The detailed results are illustrated in Table 4. The 1σ estimated errors for the original rate signal and combined rate signal before and after KF filtering can be found in Table 4. The bandwidth of KF is set as 20 Hz.

Figure 8 shows that the noises of the input rate signals are remarkably reduced by the presented KF. The basic ideal of improving the accuracy lies in the constant or small dynamic characteristic of the input signal, which is well in accordance with the requirement of the KF model. As can be seen in Table 4, the 1σ errors are reduced by a factor of more than eight by the KF, which demonstrates a considerable noise reduction for the gyroscope.

Figure 8. Plot of virtual gyroscope test with constant input rate on the turntable.

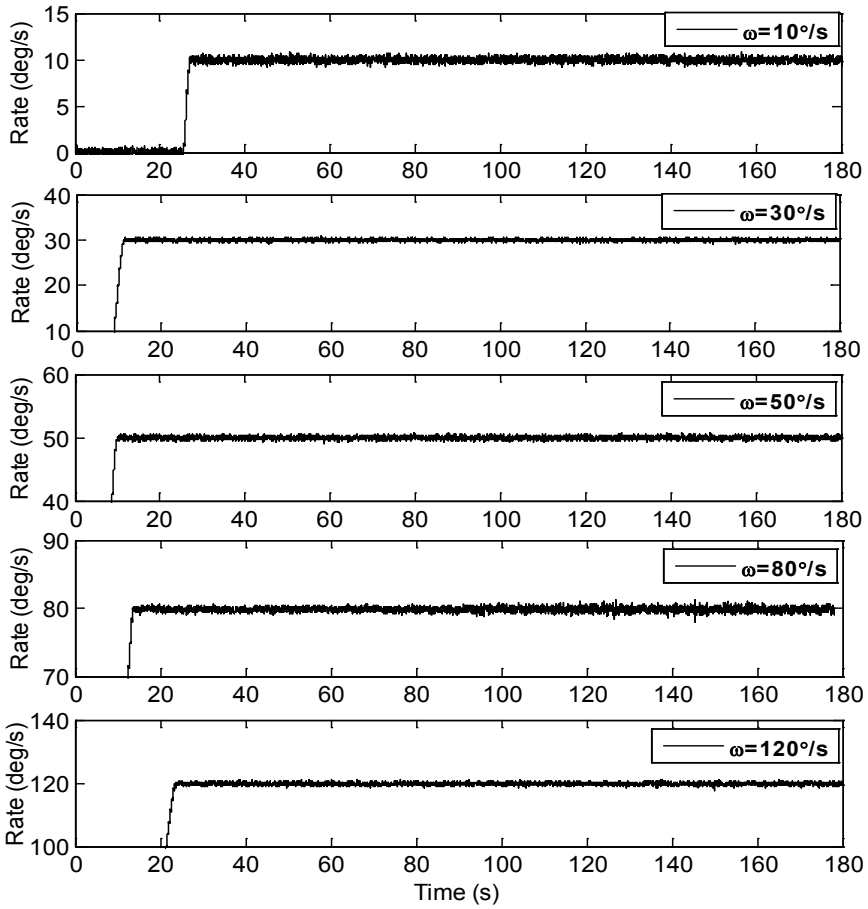

Table 4. Constant rate test results of virtual gyroscope.

Input rate ω (°/s)	Estimated error 1σ (°/s)		Improvement factor *IF*
	Single gyro	Virtual gyro	
10	2.0094	0.2027	9.9132
30	2.0189	0.2015	10.0194
50	2.0391	0.2063	9.8841
80	2.5253	0.2743	9.2063
120	2.9225	0.3395	8.6082

5.2. Swing Rate Signal Test

In the swing rate signal test, maybe the random walk model cannot reflect the sinusoidal signal well; here we try to use the random walk model to describe the input rate signal to meet the majority application. The swing rate signal test was carried out to only evaluate the ability of KF for reducing the noise and reproducing the dynamic characteristic of the input signal.

The input rate signal was set as $\omega = 10 \cdot \sin(2\pi ft + \varphi_0)$°/s with the three frequencies f = 0.1, 0.3, and 0.5 Hz, and initial phase $\varphi_0 = 0$. The comparison of the outputs of component gyroscopes and virtual gyroscope is shown in Figure 9. The results are illustrated in Table 5, where the bandwidth of KF is set as 20 Hz. The 1σ estimated errors for the angular rate signal can be found in Table 5.

Figure 9 indicates that the combined rate signal could reproduce the dynamic characteristic of the input signal well. The swings test results (Table 5) illustrate that the amplitude of the virtual gyroscope signal combined with the KF nearly reaches 10.5°/s, which is basically in accordance with the experimental setting of 10°/s without larger attenuation. Here the term "attenuation" means that the amplitude of the combined rate signal obtained by the KF is smaller than that of the original input rate signal in the dynamic test, because if the choice of q_ω accurately or closely reflects the dynamic characteristics of the input rate signal, the KF will reach the best performance, and the virtual gyroscope signal with the best accuracy can be obtained; while if q_ω were smaller than this "value", it would result in a signal attenuation, and the performance of the KF would be degraded. Furthermore, the 1σ errors are reduced from 1.6°/s to 0.30, 0.47 and 0.48°/s for the input rate signal with different frequencies, which are much smaller than that of the single devices in the array. Additionally, it indicates an increase of 1σ errors with increasing frequency *f*. This is because the dynamic characteristics of input rate signals increases with increasing frequency *f*, resulting in a larger model error for KF.

Table 5. Swing rate test results of the virtual gyroscope.

Frequency *f* (Hz)	Single gyro (°/s)		Virtual gyro (°/s)		Improvement factor (*IF*)		
	amplitude	1σ error	amplitude	1σ error	experiment	simulation	error (%)
0.1	12.4463	1.5724	10.5238	0.3023	5.2015	4.9252	5.6099
0.3	12.5270	1.6121	10.6258	0.4767	3.3818	3.6660	7.7523
0.5	12.6268	1.6954	10.6293	0.4858	3.4899	3.2357	7.8561

Figure 9. Swing rate test results of the virtual gyroscope for the input rate signals with various frequencies. **(a)** $f = 0.1$ Hz. **(b)** $f = 0.3$ Hz. **(c)** $f = 0.5$ Hz.

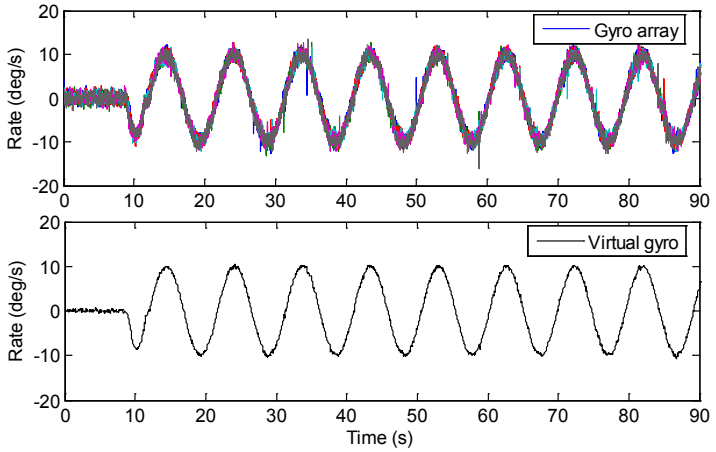

(**a**)

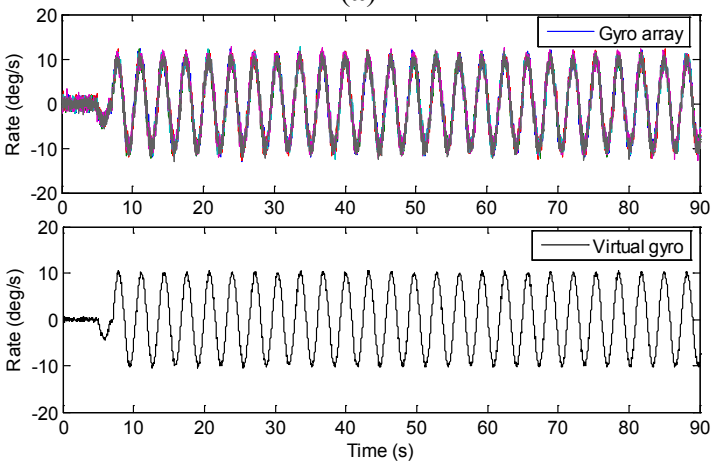

(**b**)

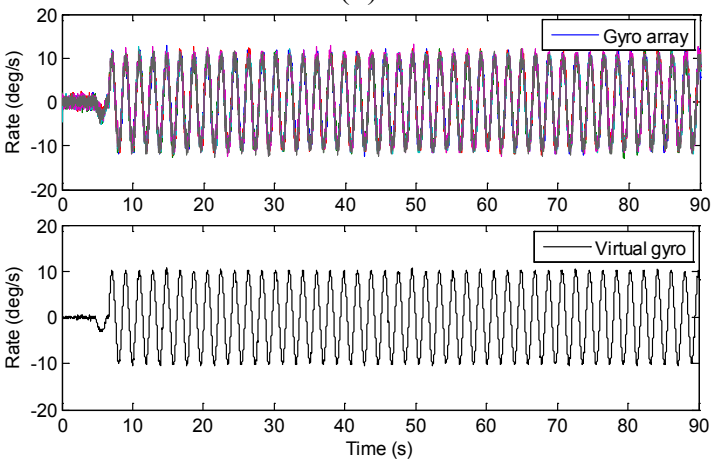

(**c**)

6. Conclusions

In this paper, the dynamic performance of the KF was analyzed to improve the accuracy of a MEMS gyroscope by combining the multiple measurements of a gyroscopes array. Six MEMS gyroscopes with the same specification were used to construct a virtual system. It displayed a 1σ noise of 0.2°/s for the combined rate signal in the constant rate test, which reduced the noise by a factor of more than eight

compared to the single gyroscope in the array. It also showed that the combined rate signal could reproduce the dynamic characteristic of the input rate signal in the dynamic condition.

Acknowledgments

The authors gratefully acknowledge the Chinese University Science Foundation's financial support (Contract No. 2014QNJJ024). Finally, the authors wish to thank the referees for their valuable comments that improved this paper.

Author Contributions

Liang Xue made substantial contributions to conception and design of the KF algorithm in this study. Lixin Wang performed the experiments and designed the system. Tao Xiong analyzed the experimental data. Chengyu Jiang and Weizheng Yuan wrote the paper.

Conflicts of Interest

The authors declare no conflict of interest.

References

1. Guo, Z.Y.; Lin, L.T.; Zhao, Q.C.; Cui, J.; Chi, X.Z.; Yang, Z.C.; Yan, G.Z. An electrically decoupled lateral-axis tuning fork gyroscope operating at atmospheric pressure. In Proceedings of the IEEE 22nd International Conference on Micro Electro Mechanical Systems, Sorrento, Italy, 25–29 January 2009; pp. 104–107.
2. Yazdi, N.; Ayazi, F.; Najafi, K. Micromachined inertial sensors. *Proc. IEEE* **1998**, *86*, 1640–1659.
3. Nitzan, S.; Ahn, C.H.; Su, T.-H.; Li, M.; Ng, E.J.; Wang, S.; Yang, Z.M.; O'Brien, G.; Boser, B.E.; Kenny, T.W.; Horsley, D.A. Epitaxially-encapsulated polysilicon disk resonator gyroscope. In Proceedings of the IEEE 26th International Conference on Micro Electro Mechanical Systems, Taipei, Taiwan, 20–24 January 2013; pp. 625–628.
4. Pakniyat, A.; Salarieh, H. A parametric study on design of a microrate-gyroscope with parametric resonance. *Measurement* **2013**, *46*, 2661–2671.
5. Mariani, S.; Ghisi, A.; Corigliano, A.; Martini, R.; Simoni, B. Two-scale simulation of drop-induced failure of polysilicon MEMS sensors. *Sensors* **2011**, *11*, 4972–4989.
6. Sonmezoglu, S.; Alper, S.E.; Akin, T. An automatically mode-matched MEMS gyroscope with 50 Hz bandwidth. In Proceedings of the IEEE 25th International Conference on Micro Electro Mechanical Systems, Paris, France, 29 January–2 February 2012; pp. 523–526.
7. Wang, W.; Lv, X.; Sun, F. Design of a novel MEMS gyroscope array. *Sensors* **2013**, *13*, 1651–1663.
8. Kim, S.; Chun, K. A gyroscope array with capacitive detection. *J. Korean Phys. Soc.* **2002**, *40*, 595–600.
9. Tanenhaus, M.; Carhoun, D.; Geis, T.; Wan, E.; Holland, A. Miniature IMU/INS with optimally fused low drift MEMS gyro and accelerometers for applications in GPS-denied environments. In Proceedings of IEEE Symposium on Position, Location and Navigation, Myrtle Beach, SC, USA, 23–26 April 2012; pp. 259–264.

10. Al-Majed, M.I.; Alsuwaidan, B.N. A new testing platform for attitude determination and control subsystems: Design and applications. In Proceedings of the IEEE/ASME International Conference on Advanced Intelligent Mechatronics, Singapore, Singapore, 14–17 July 2009; pp. 1318–1323.
11. Bayard, D.S.; Ploen, S.R. High accuracy inertial sensors from inexpensive components. U.S. Patent US20030187623A1, 2 October 2003.
12. Chang, H.; Xue, L.; Qin, W.; Yuan, G.; Yuan, W. An integrated MEMS gyroscope array with higher accuracy output. *Sensors* **2008**, *8*, 2886–2899.
13. Xue, L.; Jiang, C.Y.; Chang, H.L.; Yang, Y.; Qin, W.; Yuan, W.Z. A novel Kalman filter for combining outputs of MEMS gyroscope array. *Measurement* **2012**, *45*, 745–754.
14. Chang, H.L.; Xue, L.; Jiang, C.Y.; Kraft, M.; Yuan, W.Z. Combining numerous uncorrelated MEMS gyroscopes for accuracy improvement based on an optimal Kalman filter. *IEEE Trans. Instrum. Meas*. **2012**, *61*, 3084–3093.
15. Colomina, I.; Giménez, M.; Rosales, J.J.; Wis, M.; Gomez, A.; Miguelsanz, P. Redundant IMUs for precise trajectory determination. In Proceedings of the 20th ISPRS Congress, Istanbul, Turkey, 12–23 July 2004; pp. 1–7.
16. Waegli, A.; Skaloud, J.; Guerrier, S.; Parés, M.E.; Colomina, I. Noise reduction and estimation in multiple micro-electro-mechanical inertial systems. *Meas. Sci. Technol.* **2010**, *21*, 065201.
17. Wis, M.; Colomina, I. Dynamic dependent IMU stochastic modeling for enhanced INS/GNSS navigation. In Proceedings of the 5th ESA Workshop on Satellite Navigation Technologies and European Workshop on GNSS Signals and Signal Processing, Noordwijk, The Netherlands, 8–10 December 2010; pp. 1–5.
18. Stebler, Y.; Guerrier, S.; Skaloud, J.; Victoria-Feser, M.-P. The generalized method of wavelet moments for inertial navigation filter design. *IEEE Trans. Aerosp. Electron. Syst.* **2012**, *2012*, 24193.
19. Sadaghzadeh-Nokhodberiz, N.; Poshtan, J.; Wagner, A.; Nordheimer, E.; Badreddin, E. Cascaded Kalman and particle filters for photogrammetry based gyroscope drift and robot attitude estimation. *ISA Trans.* **2014**, *53*, 524–532.
20. El-Sheimy, N.; Hou, H.; Niu, X. Analysis and modeling of inertial sensors using Allan variance. *IEEE Trans. Instrum. Meas*. **2008**, *57*, 140–149.
21. Analog devices, ADXRS300. Available online: http://www.analog.com/static/imported-files/data_sheets/ADXRS300.pdf (accessed on 4 November 2014).
22. Texas Instrum, TMS320VC5416. Available online: http://focus.ti.com/docs/prod/folders/print/tms320vc5416.html (accessed on 4 November 2014).
23. Burr-Brown Products from Texas Instruments, ADS7807. Available online: http://focus.ti.com/lit/ds/symlink/ads7807.pdf (accessed on 4 November 2014).
24. Guerrier, S.; Skaloud, J.; Stebler, Y.; Victoria-Feser, M.-P. Wavelet variance based estimation for composite stochastic processes. *J. Am. Stat. Assoc.* **2013**, *108*, 1021–1030.